Afyon Kocatepe Üniversitesi Fen ve Mühendislik Bilimleri Dergisi

Afyon Kocatepe University Journal of Science and Engineering

AKÜ FEMÜBİD **17** (2017) **035203** ()
DOİ: 10.5578/fmbd.66319

AKU J. Sci. Eng. **17** (2017) **035203** (954-964)

Arastirma Makalesi/Reserach Article

Arteryel Spin Etiketleme ile Manyetik Rezonans Görüntülemede Echo-Planar Kodlama Hatalarının Manyetik Alan İzlemesi ve Gradyan Dürtü Fonksiyonu ile Düzeltimi

Mustafa Çavuşoğlu

ETH Zurich, Information Technology and Electrical Engineering Department, Institute for Biomedical Engineering, 8092, Zurich, Switzerland

e-posta: cavusoglu@biomed.ee.ethz.ch

Geliş Tarihi:19.07.2017 ; Kabul Tarihi:21.12.2017

Anahtar kelimeler
Arteryel Spin Etiketleme; Manyetik Alan İzlemesi; Gradyan; Düzeltme

Özet

Arteryel spin etiketleme (ASE) tabanlı perfüzyon manyetik rezonans görüntüleme tekniği çok düşük sinyal-gürültü oranına sahiptir. Dolaysıyla bu yöntem k-uzayı verisinin hızlı bir şekilde toplanmasını gerektirir. Bu genellikle veri-okuma sekansı olarak gradyan-echo EPI kullanılarak sağlanır. Bu hızlı k-uzayı geçişi, gradyanların sistem kapasitesinin limitlerinde çalışmasını ve veri toplama sırasında çok hızlı yön değiştirmelerini gerektirir ve bu gereklilik gradyan alanlarında sapmalara sebep olur. Gradyan alanlarının zamana göre değişimlerinde meydana gelen bu sapmalar görüntü oluşturmada önemli hatalar ortaya çıkmasına neden olur. Bu çalışmada, gradyan alanlarının oluşumları dinamik bir manyetik alan kamerası ile doğrudan ölçülerek ASE görüntüleri asıl gradyan alanları kullanılarak yeniden oluşturulmuştur. Bununla beraber, gradyan sisteminin doğrusal ve zamanla-değişmez bir sistem olduğu varsayılarak gradyan dürtü fonksiyonu (GDF) tanımlanabilir. Tanımlanan GDF, bir defaya mahsus bir kalibrasyon yöntemi olarak asıl gradyan şekillerinin kestirimlerinin yapılmasında ve bu kestirimler yardımı ile görüntü oluşturulmada kullanılabilir. Ek olarak ASE görüntüleri, GDF ile kestirimi yapılmış gradyan alanları kullanılarak yeniden oluşturulmuştur. Gradyan alanı sapmalarının nicel perfüzyon manyetik rezonans görüntülerine olan etkileri araştırılmıştır.

Correcting the Echo-Planar Image Encoding Imperfections in Arterial Spin Labeling MRI using Magnetic Field Monitoring and Gradient Impulse Responses

Keywords
Arterial Spin Labeling; Magnetic Field Monitoring; Gradient; Correction

Abstract

Arterial spin labeling (ASL) based perfusion MRI has inherently very low signal-to-noise ratio (SNR). Therefore, these methods require rapid k-space coverage. This is often achieved by using a readout sequence such as gradient-echo-EPI. However, such a fast k-space traversal typically needs the gradients to be operated at the maximum of the hardware specks and to be alternated rapidly during the execution which makes acquisition highly sensitive to gradient field deviations. The resulting deviations in the gradient field time courses cause substantial artifacts on the reconstructed images. In this work, we directly recorded the gradient waveform fidelities using a dynamic field camera technology and reconstructed the acquired ASL data with monitored gradient waveforms. Furthermore, by assuming that the gradient chain is a linear time-invariant (LTI) system that enables to define the gradient impulse response function (GIRF) of the system as a one-time calibration procedure, the actual gradient waveforms can be predicted. We therefore additionally performed the reconstruction based on such GIRF-predicted k-trajectories. The ultimate effects of gradient field deviations on to the absolute perfusion maps were explored.

1. Introduction

Perfusion is defined as the action of alimentative delivery of arterial blood into a certain capillary bed. It is a crucial physiological quantity for proper maintenance of normal metabolic rates as the supply of energy and the clearance of waste products. Furthermore, cerebral blood flow (CBF) is a fundamental component of the brain activity revealing the complicated neurobiology of the healthy and diseased brain functions (Buxton, 2002). Abnormalities of perfusion account for the major causes of clinical disorders, brain malfunction and mortality. Therefore, measurement of the cerebral blood flow provides key info about the tissue metabolism, vitality and function (Brown et al., 2007).

Arterial spin labeling (ASL) is a non-invasive way of quantitatively measuring the regional cerebral blood flow (rCBF) by treating the water in the arterial blood as an endogenous diffusible tracer (Detre et al., 1992). The quantitative and reproducible nature of ASL with a rapid repeatibility yielding a high temporal resolution enables to use it for functional MRI (fMRI) studies as a potential biomarker in assessing the CBF based hemodynamic response of the brain (Cavusoglu et al., 2012a).

Although ASL-MRI has already been used as a standard tool in measuring the rCBF, it has intrinsically very low signal-to-noise ratio (SNR) because perfusion replaces only ~1% of the tissue water with arriving blood water per second in gray matter (Alsop et al., 2015). Therefore, require fast k-space coverage is needed which is often accomplished by using gradient echo-planar imaging (EPI) as the read out sequence (Liu and Brown, 2007).

Fast EPI encoding requires the gradients to be executed at the physical limits of the hardware capabilities such as maximum gradient strength and to be alternated rapidly during the image acquisition (high slew rate) . A generic problem to such EPI acquisitions is their vulnerability to gradient system imperfections. The major mechanisms modulating the temporal dynamics of the gradient waveforms are bandwidth limitations of the gradient amplifiers, eddy currents generated in the conducting structures (Boesch et al., 1991; Liu et al., 1994), timing instabilities among the gradient and receive chain, mechanical vibrations of the gradient coils due to the switching (Wu et al., 2000). In practice, any deviation from the nominal gradient waveforms will disrupt the local field leading to confounds and sensitivity loss and ultimately cause substantial artifacts on the reconstructed image (Vannesjo et al., 2016). Furthermore, perfusion images are calculated based on a series of control and tag images that are often repeatedly acquired for a number of delay times (TI) to sample the ASL kinetic curves for quantifying the absolute CBF. External field fluctuations or thermal changes of the gradient system (Foerster et al., 2005) can cause actual k-space trajectories to vary over time and each of the ASL images may thus associate with particular k-space trajectories which are prone to deviate from the nominal one.

Recently, magnetic field recording using nuclear magnetic resonance (NMR) field sensors was developed to be able to monitor and correct for spatio-temporal magnetic field fluctuations (De Zanche et al., 2008). Specifically, magnetic field recording provides the actual spatio-temporal evolution of the gradient fields simultaneously with image acquisition (Barmet et al., 2008; Barmet et al., 2009). This allows to capture the dynamic effects of the eddy currents, temperature related field drifts and state changes of the gradient system during k-space encoding. Associating with those monitored field dynamics at the reconstruction level by generalizing the traditional Fourier perspective allows for accounting the effects of higher order fields terms besides global and linear k-space coefficients (Wilm et al., 2017; Wilm et al., 2015).

An efficient alternative to field monitoring is to characterize the gradient system by defining its complete impulse response function by sticking to the assumtion that the gradient chain is a linear and time-invariant (LTI) system (Vannesjo et al., 2013). Relying on the linear system theory, an absolute gradient impulse response function (GIRF) can represent the LTI terms of the field fluctuations

including amplifier and coil behaviours together with eddy currents and mechanical vibrations (Vannesjo et al., 2014). Such an approach form a basis for advanced pre-emphasis that ultimately serves to predict the effective k-space trajectories as a one-time calibration procedure (Vannesjo et al., 2013).

In this work, we studied the effects of gradient field deviations driven encoding field errors on to the absolute perfusion weighted images. We used concurrent magnetic field monitoring by deploying a dynamic field camera to study and correct for the field imperfections in EPI trajectories and time series in ASL imaging and reconstructed the ASL data with monitored gradient waveforms. Furthermore, we additionally performed the image reconstruction using GIRF-predicted k-space trajectories. To this end, we assessed its benefits for common single shot ASL sequences with EPI readout in vivo.

2. Materials and Methods

2.1. Imaging experiments

All imaging experiments were carried out on a 3T Philips Achieva system (Philips Healthcare, Best, The Netherlands) equipped with an 8-channel head receive array (Nova Medical, Wilmington, USA). Four healthy subjects (2 male, mean age 25 ± 4 y) were imaged after written informed consent based on local ethics regulations. ASL data was obtained using single-shot EPISTAR sequence (echo-planar MR imaging and signal targeting with alternating radiofrequency) including Q2TIPS modification (Edelman and Chen, 1998; Luh et al., 1999). The labeling slab was positioned at a 10 mm gap proximal to the imaging region with a width of 130 mm. The imaging region was hitted by 2 pre-saturation pulses to minimize the static tissue signal followed by a C-shaped frequency offset controlled inversion (FOCI) pulse (Yongbi et al., 1998). Other relevant sequence parameters were: FOV 220 mm2, voxel size 3 mm isotropic, TE=17 ms, TR=4 s, 5 slices, ascending slice order, averages = 30. To span the ASL kinetic curve, five inversion times were used ranging (TI=100, 500, 900, 1200, 1700 ms). To position the ASL labeling plane located perpendicular to the carotid and vertebral arteries, we additionally acquired a time-of-flight angiogram for each subject. To perform absolute perfusion quantification, M_0 images were obtained using the same protocol except ASL preparation. A spin-warp multiple-gradient-echo data were acquired to calculate the coil sensitivity and static ΔB_0 maps (TE1 = 4 ms, ΔTE= 1 ms, TR = 800 ms, 1 mm in-plane resolution) that were acquired for the same geometry. The gradient mode was set to its maximum yielding a gradient strength of 80 mT/m and with a slew rate of 100 mT/m/ms yielding a minimum TE of 17 ms.

For all MR experiments, the acquisition was simultaneously recorded using the dynamic field camera yielding the actual encoding fields (Barmet et al., 2008). Figure 1 illustrates the data acquisition and the readout schemes following the PASL module. The field probes were excited 3 ms before the onset of the respective EPI readout using a 90˚ block pulse. The received NMR signals were than sampled at 1 MHz bandwidth fully concurrently with the image acquisition.

2.2. Spatiotemporal field monitoring

To monitor the encoding fields played out by the scanner during the image readout, the NMR field probes were triggered before the pre-phaser of the EPI gradient as described in previous 3T implementations (Barmet et al., 2008; Barmet et al., 2009). The concept of spatiotemporal field monitoring is briefly summarized here.

The phase of the signal generated at a certain NMR field probe is proportional to the integral of the overall magnetic field it experiences since excitation and given as

$$\varphi(t) = \gamma \int_0^t B(\bar{r}_p, \tau)\, d\tau + \varphi_0 \qquad (1)$$

where $\bar{r}_p$ depicts the probe position, φ_0 is the initial phase after excitation and $B(\bar{r}_p, \tau)$ is the magnetic field at the probe position at a certain time which can be calculated by taking the time-derivative of the phase of the signal as

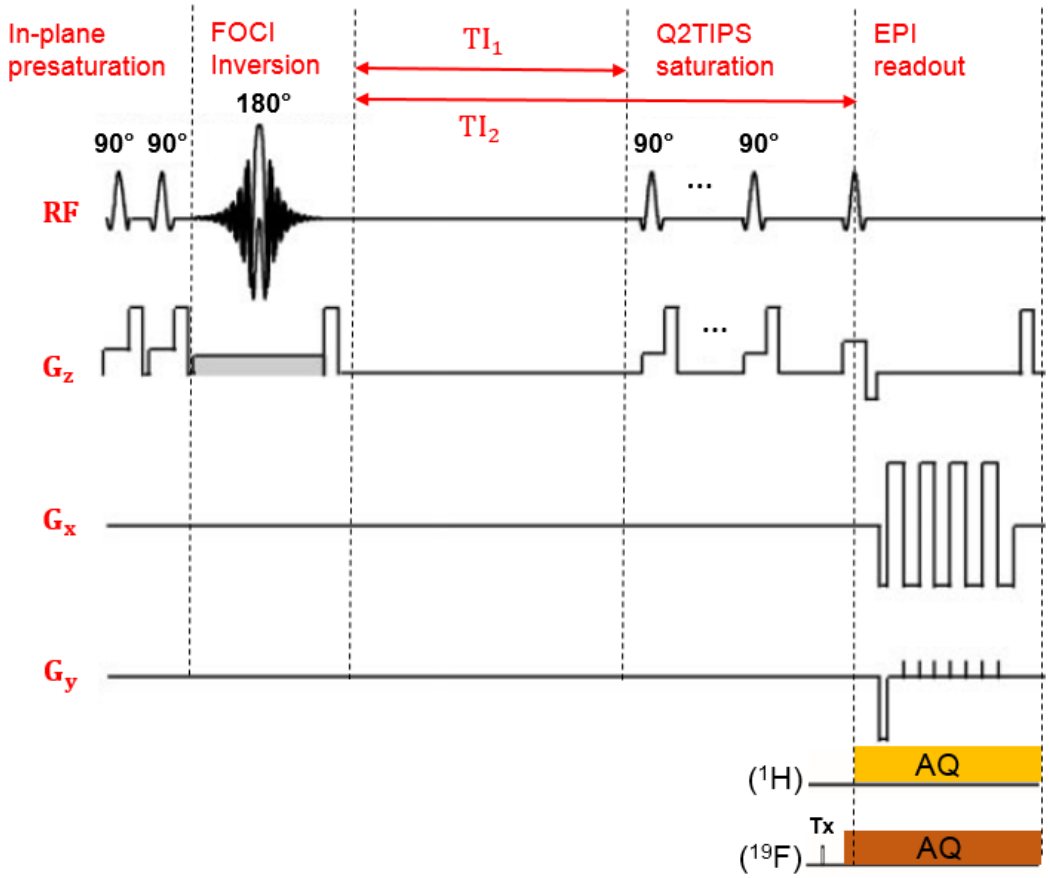

Figure 1. Sequence schematics. NMR probe array is excited before EPI prephaser. The probe field evolution is concorrently recorded with image acquisition

$$\omega(t) = \gamma . B(\bar{r}_p, t) \tag{2}$$

The local measurement of the magnetic field with a single probe can then be extended to the spatial distribution by utilizing a number of discretely localized NMR field probes assuming a smooth field distribution approximated by spatial basis functions:

$$B(\bar{r}, t) \approx \sum_i c_i(t) . b_i(\bar{r}) \tag{3}$$

where $c_i(t)$ denotes the dynamic coefficients of the spatial basis functions $b_i(\bar{r})$ reflecting their individual contribution to the overall magnetic field distribution. Since the time integral of the field coefficient $c_i(t)$ yields the phase coefficients $k_i(t)$ such that

$$k_i(t) = \gamma \int_0^t c_i(\tau) d\tau \tag{4}$$

the phase of the signal from a probe array distributed around a volume can be defined as:

$$\varphi_p(t) = \gamma \sum_i k_i(t) . b_i(\bar{r}_p) \tag{5}$$

which than can be expressed as a matrix-vector notation such as

$$\bar{\varphi}(t) = \mathbf{P}\bar{\mathrm{k}}(t) \tag{6}$$

Equation 5 implies that given a set of spatial basis functions, measuring the signal phase for a probe array at known locations yields the phase coefficients $k_i(t)$.

Field monitoring was achieved with an array of 16 transmit/receive NMR field probes operating at ^{19}F frequency (diameter: 0.8 mm, $T_1 \approx 70$ ms, $T_2^* \approx 50$ ms). A 90° block pulse was used to excite the probe

array and the NMR signals were acquired using a stand-alone spectrometer. To synchronize the ^{1}H and ^{19}F signal acquisitions, the scanner spectrometer's clock was locked to that of monitoring spectrometer. The probe placement was performed on to a spherical surface for appropriate conditioning of the spherical harmonic field expansions.

The probe signal was processed by performing demodulation, phase extraction and phase unwrapping. In this expansion, the 0th order term k_0 corresponds to a global phase whereas 1st order term k_x, k_y, k_z represent the linear phase terms. Only the 0th and 1st order k-space coefficients were considered in image reconstruction.

2.3. Gradient impulse response function (GIRF) estimation

Alternative to direct field camera measurements of the gradient waveforms, it is possible to define the GIRF of the system by assuming that the gradient chain is a linear and time-invariant system (Vannesjo et al., 2013). The GIRF of the system can be calculated by deconvolving the measured output waveform with its known input waveform. Because GIRF is frequency dependent, the input waveform used in the measurement should ideally involve all frequencies in the bandwidth of interest. In principle, the most appropriate input function for such a task would be a dirac-delta function covering an infinite bandwidth. However, due to the practical challenges in physical realization of such a function as an input to the gradient system, linear frequency-swept pulses (chirp pulses) were used instead as an input to properly encode the varying frequencies in the bandwidth (Vannesjo et al., 2014). During the measurements to obtain the GIRF, the same dynamic field camera and associated software was used. For all experiments, the standard gradient pre-emphasis system to compensate for eddy currents was turned on.

2.4. MR Image Reconstruction

Figure 2 illustrates the key ingredients of the MR image reconstruction as a framework including monitored or GIRF estimated encoding fields, coil sensitivities and static ΔB_0 maps. The raw image signal $s_\beta(t)$ acquired with coil β at time t is expressed as

$$s_\beta(t) = \int m(\boldsymbol{r}).c_\beta(\boldsymbol{r}).e^{i\varphi(\boldsymbol{r},t)}e^{i\Delta\omega(\boldsymbol{r})t}d\boldsymbol{r} \qquad (7)$$

where $m(\boldsymbol{r})$ denotes the transverse magnetization as function of spatial position $\boldsymbol{r}$, $c_\beta(\boldsymbol{r})$ denotes the sensitivity of coil β, $\varphi(\boldsymbol{r},t)$ denotes the phase model obtained by field monitoring and $\Delta\omega(\boldsymbol{r})$ denotes the static off-resonance. The discretized MR signal can then be expressed as

$$s_{(\beta,\tau)} = \sum_{\rho=1}^{N_\rho} m_\rho.\exp(ik_0(t_k))E_{(\beta,\tau),\rho} \qquad (8)$$

where $\boldsymbol{m} = (m_1,\dots,m_\rho,\dots,m_{N_\rho})$ represents the discretized object magnetization, τ,ρ are index terms in time and space, respectively. The effects of the 1st order field terms and the static off-resonance was included in the Fourier encoding matrix $\boldsymbol{E}$ which is defined as

$$E_{(\beta,\tau),\rho} = c_\beta(\boldsymbol{r}_\rho).e^{i(k_0(t_\tau)+\boldsymbol{k}(t_\tau).\boldsymbol{r})}.e^{i\Delta\omega(\boldsymbol{r}_\rho)t_\tau} \qquad (9)$$

The image reconstruction and subsequent data analysis steps were performed in Matlab (The Mathworks, Natrick, MA) on a CPU cluster. The inversion of the Eq.6 was implemented using the conjugate-gradient method based on gridding (Pruessmann et al., 2001). A spin-warp multiple-gradient-echo images were acquired and reconstructed by incorporating with the monitored phase coefficients to obtain the coil sensitivities $c_\beta(\boldsymbol{r})$ and static off-resonance maps $\Delta\omega(\boldsymbol{r})$.

2.5. Perfusion quantification

The ASL data was pre-processed using the FSL software (http://www.fmrib.ox.ac.uk/fsl) and in-built MATLAB (The Mathworks, Natick, MA, USA) scripts (Smith et al., 2004). MCFLIRT module of FSL was used to motion correct the time courses of all voxels (Jenkinson et al., 2002). For co-registration, the mean image of each session was used as

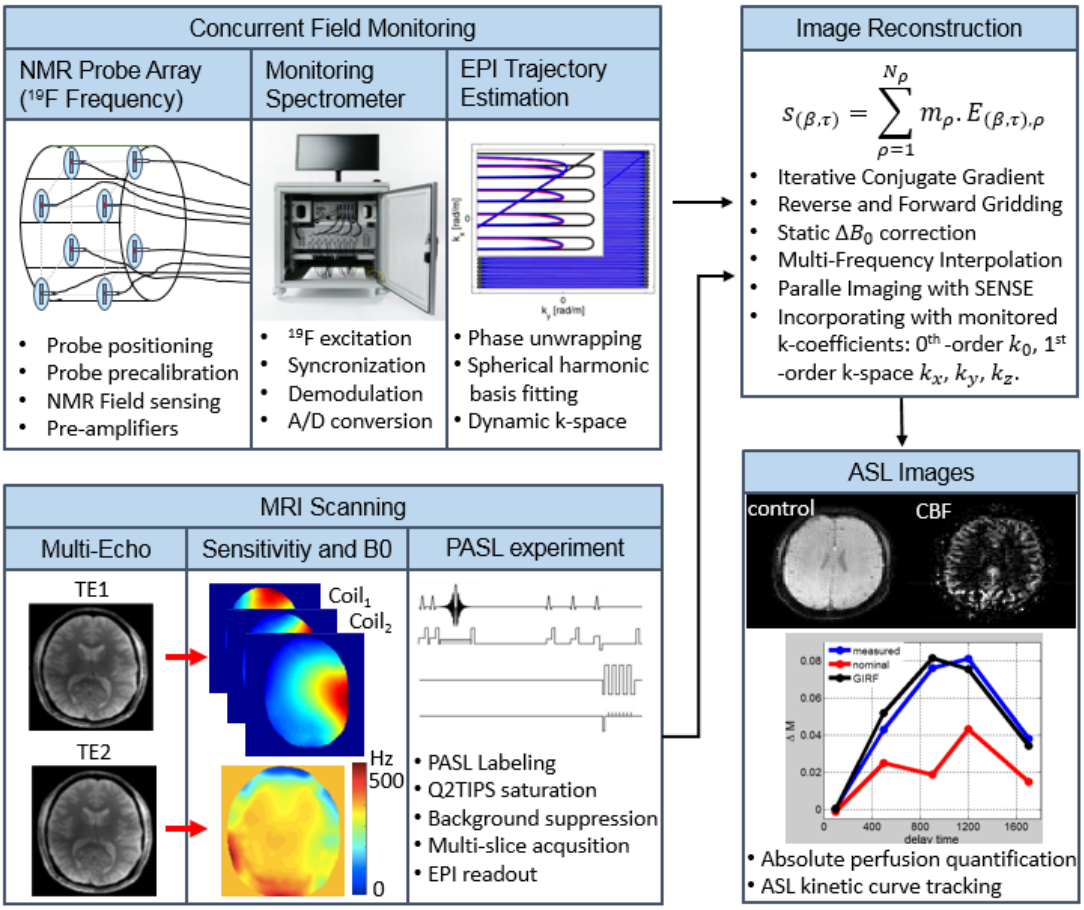

Figure 2. Image formation based on the proposed framework

reference. Absolute perfusion quantification was according to the procedure described in detail in references (Alsop et al., 2015; Cavusoglu et al., 2009) where the labeling efficiency was taken as 0.98, blood T_1 was assumed to be 1650 ms, partition coefficient was taken as 0.9 mL/g. Kinetic curves were computed for each voxel from the set of the averaged perfusion images using the standard kinetic model (Buxton et al., 1998). The actual inversion time of each slice was computed and applied for slice scan time correction (Cavusoglu et al., 2012b).

3. Results

The applied chirp pulses to compute the GIRFs and their corresponding frequency responses over the full bandwidth were plotted in Figure 3.a-b respectively. Figure 3.c-d illustrates the magnitude and the phase plots of the GIRFs for different gradient directions that are measured using the dynamic field camera. The frequency resolution was 167 Hz for the system dictated by the duration of the chirps (6ms). The low-pass filter behavior of the gradient system is observable demonstrating that at lower frequencies, the eddy current compensation broadens the response plateau. Moreover, a common feature about the GIRF is that x and y gradient axes results very similar responses. In contrast, z gradient has a slightly narrower

bandwidth at full width at half maximum (FWHM). Figure 3.d shows that there is almost-zero net delay in all gradient channels reflected by the flatness of the phase patterns around DC (zero frequency) implying an appropriate delay calibration was performed.

Figure 4.a show a comparison of the 0th order phase coefficient (k_0) mentioning that the trajectories predicted by using the GIRFs reflects many features of the actual k-space trajectory and precisely predicts fluctuations in k_0 due to the readout gradient. A time-linear component observed in the concurrently monitored k_0, but not in the GIRF prediction, arises from lower-order concomitant field terms. As concomitant fields scale non-linearly with the gradient strength, they cannot be predicted by the GIRF approach. Figure 4.b provides a comparison between ideal, monitored and GIRF estimated trajectories for the EPI acquisitions. The monitored trajectory deviates substantially from the ideal trajectory especially at the switching. The trajectory estimated by using GIRF closely follows the monitored trajectory with slight differences. The difference between GIRF-predicted and the measured trajectory in the readout direction is around 40 rad/m implying that the demanded image resolution is slightly higher than that of achieved.

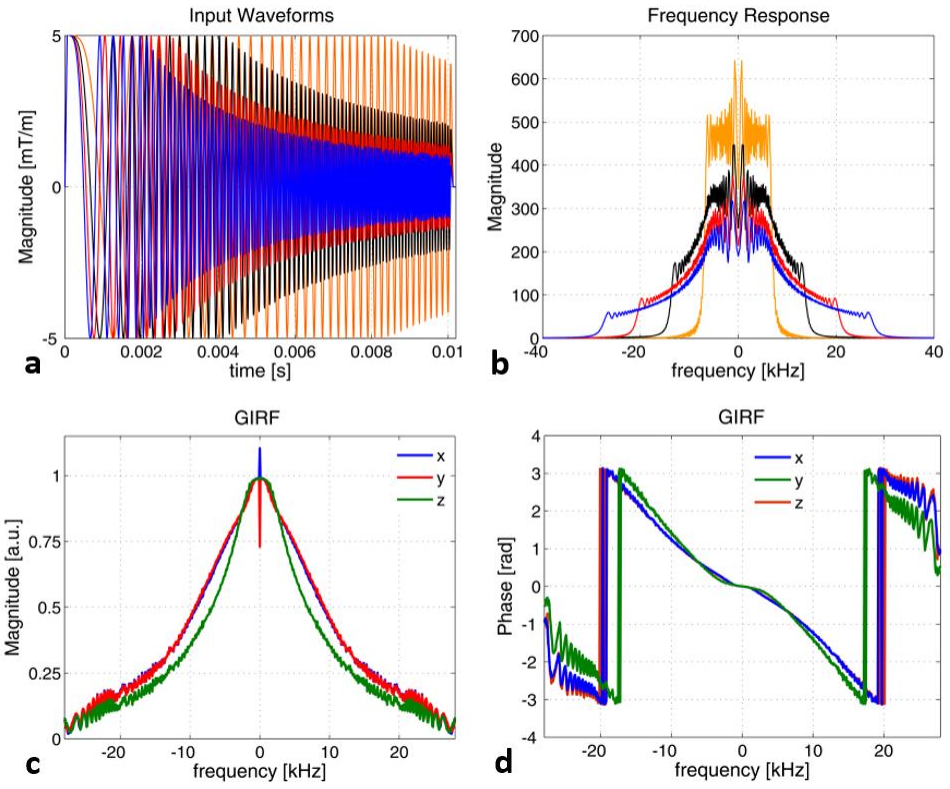

Figure 3.a. Chirp pulses that were used as an input to compute the GIRF **b.** The frequency response of the system to the applied chirp pulses **c.** The magnitude plots of the GIRF in all directions **d.** The phase plots of the GIRF in all directions

Figure 5 shows the reconstructed ASL control images based on ideal, GIRF estimated and monitored trajectories. The ASL control image exhibits strong ghosting artifacts based on nominal trajectory reconstruction (Figure 5.a). Reconstruction by using the using the GIRF-predicted trajectory (Figure 5.b) or concurrently monitored trajectories (Figure 5.c) largely eliminates such artifacts in reconstruction. Due to the time linear component in k_0, a shift of about 1 pixel in the phase-encoding direction is observed between the GIRF-based and the monitoring based

reconstructions. Figure 5.d-e depicts the difference images compared to the monitored reconstructions with the same intensity scale as in the reconstructed images.

Figure 6 shows the corresponding absolute perfusion-weighted images and their differences scaled to percent of the maximum value implying that trajectory errors cause very large (more than 100 %, Figure 6.d) inaccuracies in perfusion images reconstructed using the nominal trajectories Figure 6.a). These are highly eliminated in the GIRF reconstruction (Figure 6.b), which however still exhibits some discrepancy (Figure 6.e) relative to the reconstructions using concurrently monitored trajectories (Figure 6.c).

Figure 7 show the ASL kinetic curves that are calculated in a ROI by averaging involving of only gray matter voxels enclosed with a yellow circle in Figure 6.a. While the dynamics of the ASL kinetic curves obtained from images reconstructed based on the GIRF-predicted and concurrently monitored trajectories are very close to each other, CBF is significantly underestimated in all inversion time points of the kinetic curve obtained from the image reconstructed based on the nominal trajectory.

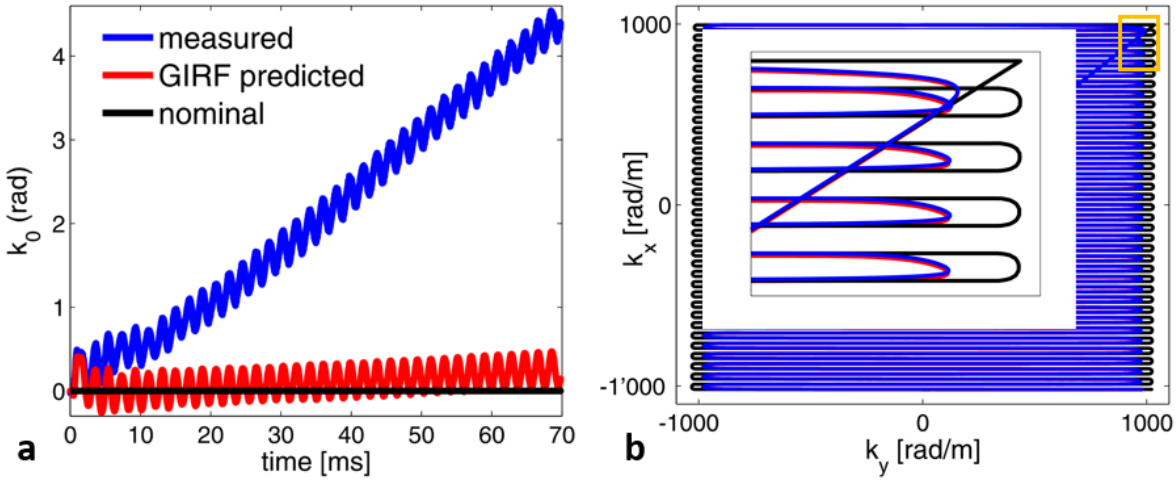

Figure 4.a Nominal, GIRF-predicted and concurrently measured zeroth-order phase coefficient (k_0) **b.** Nominal, GIRF-predicted and concurrently monitored first-order k-space trajectory in an EPI acquisition. The yellow frame is zoomed in where the monitored and GIRF-predicted trajectory deviations are clear compare to the nominal trajectory

4. Discussion and Conclusion

In this work, we investigated the effects of encoding field imperfections in an EPI readout on the quantitative perfusion-weighted imaging acquired using ASL-MRI. The k-space trajectories based on nominal, GIRF-estimation and concurrent monitoring were used for ASL image reconstruction. We found that, significant artifacts (up to 100%) can be caused by gradient field imperfections in perfusion-weighted images and we showed that concurrent field monitoring can largely eliminate these artifacts.

It was observed that the characteristics of the images reconstructed using the GIRF-predicted trajectories are comparable to using concurrent field monitoring for trajectory measurement. This is a major advantage since GIRF-based estimations are independent from the selected k-space trajectory and thus could serve as a general correction technique for reproducible field imperfection as a

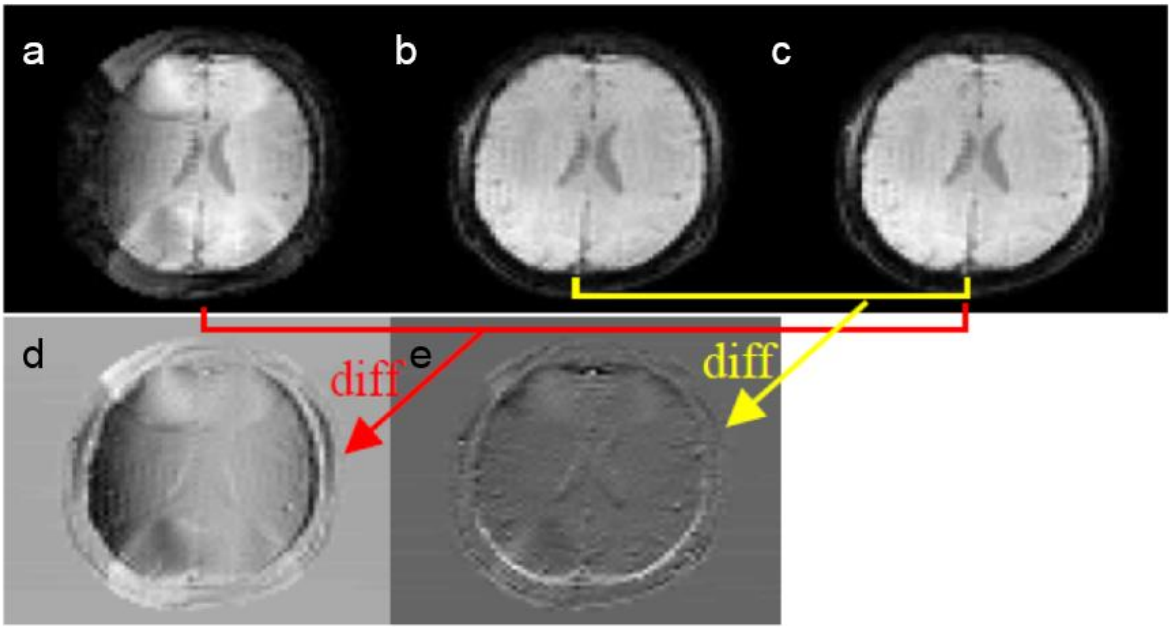

Figure 5. ASL control images reconstructed based on a. Nominal **b.** GIRF-predicted **c.** concurrently monitored k-space trajectories. To better emphasize the improvement with trajectory correction the difference images were plotted **(d-e).**

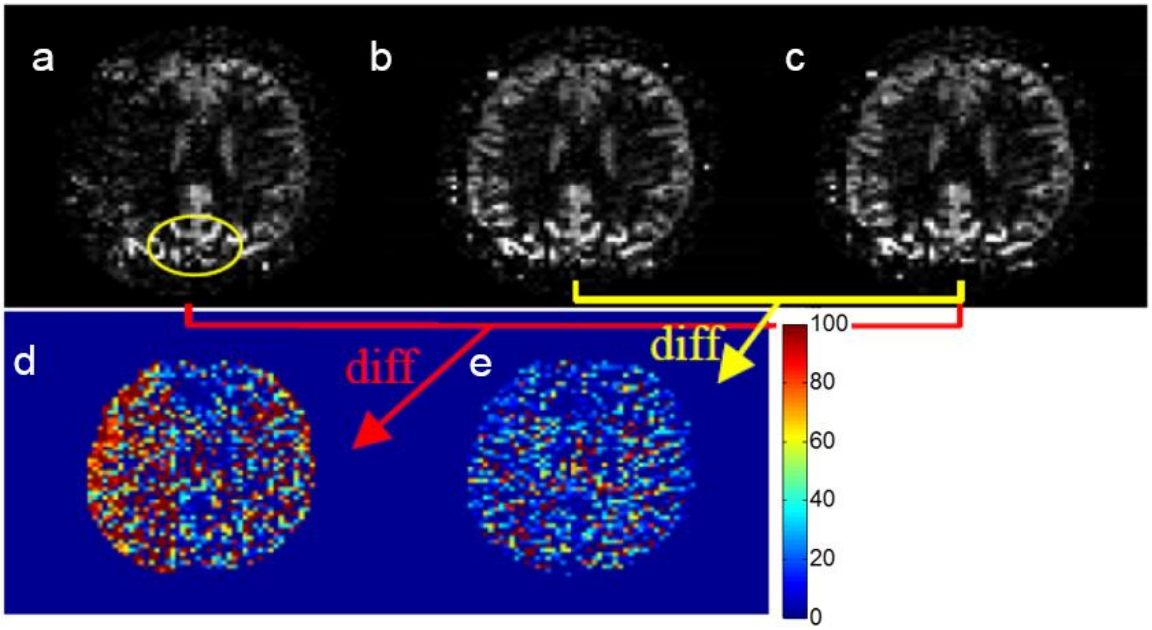

Figure 6. Absolute perfusion images calculated from the ASL images reconstructed based on **a.** Nominal **b.** GIRF-predicted **c.** concurrently monitored k-space trajectories. To better emphasize the improvement with trajectory correction the difference images were plotted **(d-e)**

one-time calibration procedure. Generally, the GIRF technique enables to correct for cross-terms in case accurately characterized. However, GIRF-approach does not count for non-linear components of gradient dynamics and fluctuations over time. For specific encoding schemes, available methods such as EPI phase correction are not adequately reliable for clinical practice and they do not cover advanced k-space encoding strategies. We here showed that GIRF-based reconstruction significantly reduces these artifacts. The remaining artifacts could be due to the higher-order cross-term responses. Note that, the GIRF method is only true with the assumption that the system is LTI. Any non-linear terms and irreproducible field fluctuations such as gradient heating causes this model to be violated. To further increase reconstruction accuracy, gradient field evolutions acquired with concurrent field monitoring can be used, at the expense of requiring a specialized hardware setup and a higher-order signal model.

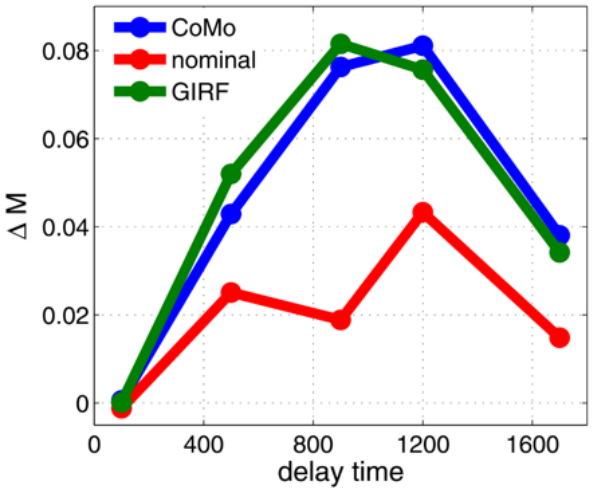

Figure 7. ASL kinetic curves calculated in a ROI labeled with a yellow circle in Figure 6.a. The kinetic curve of ASL images with nominal trajectory significantly underestimates the perfusion.

In contrast with existing trajectory correction strategies, such as EPI phase correction, both the GIRF-approach and concurrent monitoring extend to more sophisticated k-space encoding strategies. Spiral acquisitions would be particularly promising for ASL, due to their short echo-time and fast k-space coverage, but have hitherto not been feasible on most systems because of their vulnerability to trajectory imperfections. This could potentially be overcome by the use of GIRF- or monitoring-based reconstructions.

References

Alsop, D.C., Detre, J.A., Golay, X., Gunther, M., Hendrikse, J., Hernandez-Garcia, L., Lu, H.Z., MacIntosh, B.J., Parkes, L.M., Smits, M., van Osch, M.J.P., Wang, D.J.J., Wong, E.C., Zaharchuk, G., 2015. Recommended Implementation of Arterial Spin-Labeled Perfusion MRI for Clinical Applications: A Consensus of the ISMRM Perfusion Study Group and the European Consortium for ASL in Dementia. Magnetic Resonance in Medicine 73, 102-116.

Barmet, C., De Zanche, N., Pruessmann, K.P., 2008. Spatiotemporal magnetic field monitoring for MR. Magnetic Resonance in Medicine 60, 187-197.

Barmet, C., De Zanche, N., Wilm, B.J., Pruessmann, K.P., 2009. A Transmit/Receive System for Magnetic Field Monitoring of In Vivo MRI. Magnetic Resonance in Medicine 62, 269-276.

Boesch, C., Gruetter, R., Martin, E., 1991. Temporal and Spatial-Analysis of Fields Generated by Eddy Currents in Superconducting Magnets - Optimization of Corrections and Quantitative Characterization of Magnet Gradient Systems. Magnetic Resonance in Medicine 20, 268-284.

Brown, G.G., Clark, C., Liu, T.T., 2007. Measurement of cerebral perfusion with arterial spin labeling: Part 2. Applications. Journal of the International Neuropsychological Society 13, 526-538.

Buxton, R.B., 2002. Introduction to Functional Magnetic Resonance Imaging: Principles and Techniques. Cambridge University Press, Cambridge.

Buxton, R.B., Frank, L.R., Wong, E.C., Siewert, B., Warach, S., Edelman, R.R., 1998. A general kinetic model for quantitative perfusion imaging with arterial spin labeling. Magn. Reson. Med. 40, 383-396.

Cavusoglu, M., Bartels, A., Yesilyurt, B., Uludag, K., 2012a. Retinotopic maps and hemodynamic delays in the human visual cortex measured using arterial spin labeling. Neuroimage 59, 4044-4054.

Cavusoglu, M., Pfeuffer, J., Ugurbil, K., Uludag, K., 2009. Comparison of pulsed arterial spin labeling encoding schemes and absolute perfusion quantification. Magn Reson Imaging 27, 1039-1045.

Cavusoglu, M., Pohmann, R., Burger, H.C., Uludag, K., 2012b. Regional effects of magnetization dispersion on

quantitative perfusion imaging for pulsed and continuous arterial spin labeling. Magn Reson Med.

De Zanche, N., Barmet, C., Nordmeyer-Massner, J.A., Pruessmann, K.P., 2008. NMR probes for measuring magnetic fields and field dynamics in MR systems. Magnetic Resonance in Medicine 60, 176-186.

Detre, J.A., Leigh, J.S., WIlliams, D.S., Koretsky, A.P., 1992. Perfusion imaging. Magn. Reson. Med. 23, 37-45.

Edelman, R.R., Chen, Q., 1998. EPISTAR MRI: multislice mapping of cerebral blood flow. Magn. Reson. Med. 40, 800-805.

Foerster, B.U., Tomasi, D., Caparelli, E.C., 2005. Magnetic field shift due to mechanical vibration in functional magnetic resonance imaging. Magnetic Resonance in Medicine 54, 1261-1267.

Jenkinson, M., Bannister, P., Brady, M., Smith, S., 2002. Improved optimization for the robust and accurate linear registration and motion correction of brain images. Neuroimage 17, 825-841.

Liu, Q., Hughes, D.G., Allen, P.S., 1994. Quantitative Characterization of the Eddy-Current Fields in a 40-Cm Bore Superconducting Magnet. Magnetic Resonance in Medicine 31, 73-76.

Liu, T.T., Brown, G.G., 2007. Measurement of cerebral perfusion with arterial spin labeling: Part 1. Methods. Journal of the International Neuropsychological Society 13, 517-525.

Luh, W.M., Wong, E.C., Bandettini, P.A., Hyde, J.S., 1999. QUIPSS II with thin-slice TI1 periodic saturation: a method for improving accuracy of quantitative perfusion imaging using pulsed arterial spin labeling. Magn Reson Med 41, 1246-1254.

Pruessmann, K.P., Weiger, M., Bornert, P., Boesiger, P., 2001. Advances in sensitivity encoding with arbitrary k-space trajectories. Magnetic Resonance in Medicine 46, 638-651.

Smith, S.M., Jenkinson, M., Woolrich, M.W., Beckmann, C.F., Behrens, T.E., Johansen-Berg, H., Bannister, P.R., De Luca, M., Drobnjak, I., Flitney, D.E., Niazy, R.K., Saunders, J., Vickers, J., Zhang, Y., De Stefano, N., Brady, J.M., Matthews, P.M., 2004. Advances in functional and structural MR image analysis and implementation as FSL. Neuroimage 23 Suppl 1, S208-219.

Vannesjo, S.J., Dietrich, B.E., Pavan, M., Brunner, D.O., Wilm, B.J., Barmet, C., Pruessmann, K.P., 2014. Field Camera Measurements of Gradient and Shim Impulse Responses Using Frequency Sweeps. Magnetic Resonance in Medicine 72, 570-583.

Vannesjo, S.J., Graedel, N.N., Kasper, L., Gross, S., Busch, J., Haeberlin, M., Barmet, C., Pruessmann, K.P., 2016. Image Reconstruction Using a Gradient Impulse Response Model for Trajectory Prediction. Magnetic Resonance in Medicine 76, 45-58.

Vannesjo, S.J., Haeberlin, M., Kasper, L., Pavan, M., Wilm, B.J., Barmet, C., Pruessmann, K.P., 2013. Gradient system characterization by impulse response measurements with a dynamic field camera. Magnetic Resonance in Medicine 69, 583-593.

Wilm, B.J., Barmet, C., Gross, S., Kasper, L., Vannesjo, S.J., Haeberlin, M., Dietrich, B.E., Brunner, D.O., Schmid, T., Pruessmann, K.P., 2017. Single-shot spiral imaging enabled by an expanded encoding model: Demonstration in diffusion MRI. Magnetic Resonance in Medicine 77, 83-91.

Wilm, B.J., Nagy, Z., Barmet, C., Vannesjo, S.J., Kasper, L., Haeberlin, M., Gross, S., Dietrich, B.E., Brunner, D.O., Schmid, T., Pruessmann, K.P., 2015. Diffusion MRI with Concurrent Magnetic Field Monitoring. Magnetic Resonance in Medicine 74, 925-933.

Wu, Y.H., Chronik, B.A., Bowen, C., Mechefske, C.K., Rutt, B.K., 2000. Gradient-induced acoustic and magnetic field fluctuations in a 4T whole-body MR imager. Magnetic Resonance in Medicine 44, 532-536.

Yongbi, M.N., Branch, C.A., Helpern, J.A., 1998. Perfusion imaging using FOCI RF pulses. Magn. Reson. Med. 40, 938-943.